Ultrastable lasers based on vibration insensitive cavities

J. Millo, D. V. Magalhães, C. Mandache, Y. Le Coq, E. M. L. English,* P. G. Westergaard, J. Lodewyck, S. Bize, P. Lemonde, and G. Santarelli

LNE-SYRTE, Observatoire de Paris, CNRS, UPMC, 61 Avenue de l'Observatoire, 75014 Paris, France

(Received 5 February 2009; published 18 May 2009)

We present two ultrastable lasers based on two vibration insensitive cavity designs, one with vertical optical axis geometry, the other horizontal. Ultrastable cavities are constructed with fused silica mirror substrates, shown to decrease the thermal noise limit, in order to improve the frequency stability over previous designs. Vibration sensitivity components measured are equal to or better than $1.5\times10^{-11}/\mathrm{m\ s^{-2}}$ for each spatial direction, which shows significant improvement over previous studies. We have tested the very low dependence on the position of the cavity support points, in order to establish that our designs eliminate the need for fine tuning to achieve extremely low vibration sensitivity. Relative frequency measurements show that at least one of the stabilized lasers has a stability better than 5.6×10^{-16} at 1 s, which is the best result obtained for this length of cavity.

DOI: 10.1103/PhysRevA.79.053829 PACS number(s): 42.60.Da, 07.60.Ly, 42.62.Fi

I. INTRODUCTION

Ultrastable laser light is a key element for a variety of applications ranging from optical frequency standards [1,2], tests of relativity [3], generation of low-phase-noise microwave signals [4], and transfer of optical stable frequencies by fiber networks [5,6], to gravitational wave detection [7–9]. These research topics, in particular cold atoms and single-ion optical frequency standards, have stimulated new approaches to the design of Fabry-Pérot reference cavities which are used to stabilize lasers.

For optical frequency standards with neutral atoms, the frequency noise of state-of-the-art ultrastable clock lasers sets a severe limit to the clock frequency stability via the Dick effect [10]. Due to this limitation, the best reported Allan deviations are more than 1 order of magnitude larger than the ultimate quantum limit of these clocks [2]. Improving the laser frequency stability is therefore a prerequisite for approaching this quantum limit.

One important issue for reducing the frequency noise of stabilized laser cavities is to minimize the effects of residual vibration. Vibration isolation systems can minimize the noise level, but compact commercial systems are generally not sufficient to reach a subhertz laser linewidth. One way to improve the spectral performance of stabilized lasers is to reduce vibration sensitivity by carefully designing the cavity geometry and its mounting. Several groups have proposed and implemented low vibration sensitivity cavities [11–14]. A second important issue is the reduction in thermal noise in cavity elements [15]. The ultrastable cavities presented here further reduce both vibration sensitivity and thermal noise level, and therefore improve cavity stability.

The two different optical cavities are designed based on the results of extensive simulations using finite element software. The optical axis, which is also the axis of the spacer, is horizontal for one cavity (Fig. 1) and vertical for the other (Fig. 2). In each case, the position and size of the cavity support points and the effect of mirror tilt have been analyzed. The constructed cavities have then been subjected to an extensive study of the vibration response. Both cavity types exhibit extremely low vibration sensitivity. Sensitivities are equivalent to previous horizontal cavity designs [12,14] but with strongly reduced dependence on support points' position. The vertical cavity shows a much lower sensitivity than previous vertical cavity designs [13]. Moreover, a significant improvement of the thermal noise level is demonstrated here [13,16] by using fused silica mirror substrates, which minimize the contribution to thermal noise due to the higher mechanical Q factor of this material in comparison to Ultra Low Expansion glass (Corning ULE).

II. FINITE ELEMENT MODELING OF THE CAVITY

A. General considerations

This analysis is restricted to the quasistatic response of cavities as mechanical resonances are in the 10 kHz range, while only low frequencies of <100 Hz are of interest in the present experiment for application to optical atomic clocks. Furthermore, with commercial compact isolation systems the

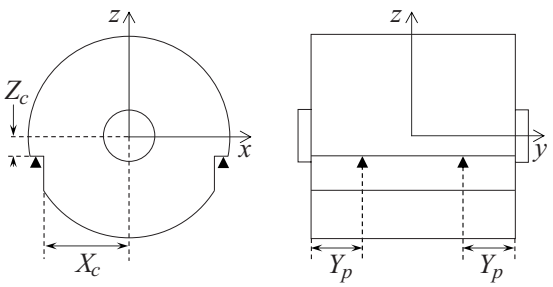

FIG. 1. Front and side views of the horizontal cavity. The optical axis lies along the y axis. The four support points are represented with black triangles. The positions of the cutouts for support points are shown: X_c with respect to the yz plane, and Z_c with respect to the xy plane. Y_p is the distance along the y axis from the end of the cavity.

*elizabeth.english@obspm.fr

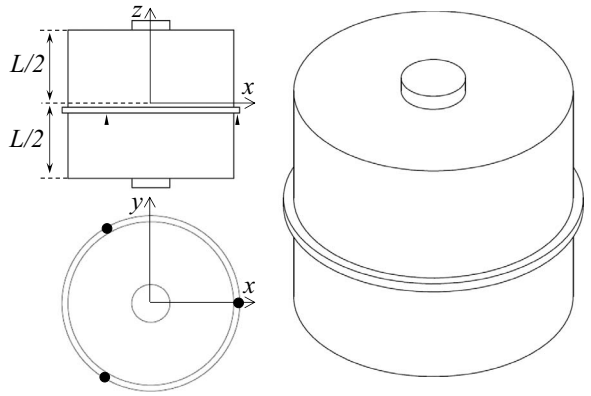

FIG. 2. Top, side, and isometric views of the vertical cavity. The optical axis is aligned to the z axis. The three support points are represented with black triangles or black circles.

vibration level is still significant below ~1 Hz where they are not effective at reducing seismic noise.

In the finite element model, spacer and mirror substrates are considered to be a single rigid body. The cavity geometry is meshed with 125 000 prism elements, where each prism has 6 nodes. Finite element deformations are calculated within the elastic limit. When the constrained cavity is accelerated, a length variation is induced by elastic deformations. Careful design of the cavity allows for compensation of this variation using Poisson's effect [17] and cavity symmetries. Deformation simulations have been done using the mechanical properties of ULE: mass density (2210 kg m^{-3}), Young's modulus (67.6 GPa), and Poisson's ratio (0.17).

Vibration sensitivity of the cavities is deduced by observing the deformation in the mirrors for a given acceleration value. The displacement of the central region (where the laser beam is reflected) is of interest in the present study. Two types of mirror deformations are important for both vertical and horizontal cavities.

The first type is the mirror translation along the cavity axis, in order to analyze the distance between mirror's centers. These length variations exist if the cavity has no symmetry plane orthogonal to the acceleration axis.

The second type is the mirror tilt (Fig. 3), where the mirrors are shifted through an angle θ. For an ideal cavity where optical and mechanical axes coincide, the tilt-induced length variation is a second-order effect and can be neglected. In a real cavity, mechanical and optical axes are not coincident due to imperfections in the construction (e.g., mirror polishing, spacer machining, and contacting of the mirrors onto the spacer). A worst case situation is considered in the present study, where the optical and mechanical axes are parallel and displaced by a distance d. The schematic in Fig. 3 illustrates the cavity deformation through mirror tilt and the optical length change from L to L'. Length variations become proportional to both d and the tilt angle. Consequently, tilt is a first-order effect on the cavity length and must therefore be considered. Note that the mirrors' tilt angle θ is extremely small in reality, so any change in the pointing direction of the optical axis that may occur would be a second-order effect of θ. Therefore these small movements in the pointing direction of the optical axis do not change L significantly.

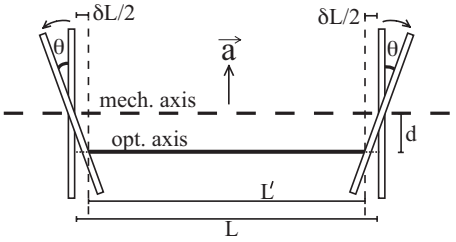

FIG. 3. Schematic showing mirror tilt as a result of applied transverse acceleration $\vec{a}$. This tilt occurs in both horizontal and vertical cavities, and leads to changes in cavity length L as the optical axis is displaced from the mechanical axis by a distance d. Note that the mirror tilt and d are exaggerated in this figure to illustrate this small effect clearly.

For the horizontal cavity under longitudinal acceleration a slightly different type of tilt configuration occurs, which will be explained later on.

We can write the cavity length variations in the following way:

$$\delta L/L = \vec{k} \cdot \vec{a}, \tag{1}$$

where $\vec{a}$ is the acceleration vector and $\vec{k}$ is the vector of vibration sensitivities where the components are expressed as

$$k_x = k_x^L + k_x^T(d),$$

$$k_y = k_y^L + k_y^T(d),$$

$$k_z = k_z^L + k_z^T(d), \tag{2}$$

where k_i^L and $k_i^T(d)$ are, respectively, the sensitivity coefficients to the mirrors' translation and tilt.

B. Horizontal cavity

The horizontally mounted optical cavity configuration is 100 mm long. For this cavity, the optical axis lies along the y axis and the spacer diameter is 100 mm (Fig. 1). The position of the four support points has been carefully calculated through extensive simulations to design a cavity with very low vibration sensitivity. The contact planes for these support points are obtained by machining two square "cutouts" along the length (y axis) of the cylindrical spacer. All four contact points are on the same horizontal plane and are placed symmetrically around the cavity as shown in Fig. 1.

Ideally, to be least sensitive to vibrations, the cavity spacer should be a perfect cylinder supported at the horizontal midplane (xy axis), with contact points located on the surface of the spacer. In this case the cavity and support points are completely symmetric and so any acceleration will not induce mirror translations.

Practically, we have assumed that a cutout shoulder of at least 3 mm is required to support the cavity effectively. Therefore most simulations were calculated using $X_c = 47$ mm (Fig. 4). Due to the cutouts breaking the cavity symmetry about the xy plane, cancellation of mirror translation due to vertical acceleration is no longer guaranteed by the symmetry. However, for some cutout geometries, a spe-

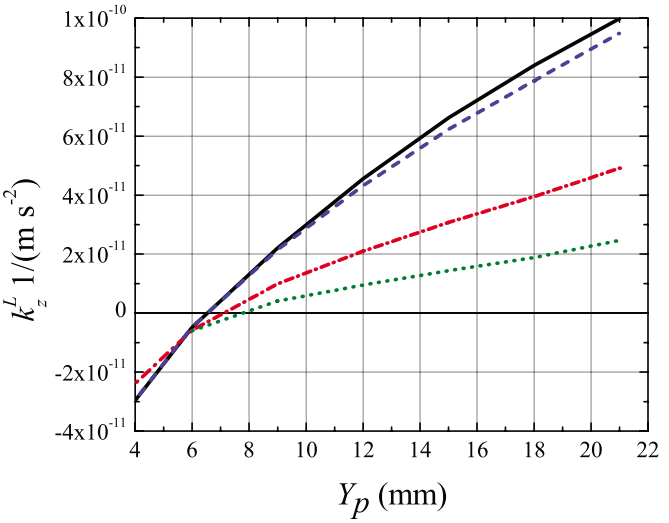

FIG. 4. (Color online) Simulation showing the slope obtained for k_z^L for different cutout geometries. For each plot, X_c=47 mm. Black solid line: Z_c=9 mm; blue dashed line: Z_c=7 mm; red dot-dashed line: Z_c=5 mm; green dotted line: Z_c=3 mm.

cific position of support points (Y_p) can be found with the simulation which suppresses mirror translations, i.e., k_z^L=0.

To make a practical adjustment of the support points' position less critical, the slope of the acceleration sensitivity k_z^L as function of the support points' position Y_p has to be minimized. Simulations show that to achieve this, the cutouts must be placed as close to the horizontal midplane (xy axis) as possible.

Unfortunately, a vanishing sensitivity to vertical acceleration k_z^L=0 cannot be achieved for every cutout geometry. Furthermore, simulations performed using two different models for the support points have shown quite different results, as can be clearly seen in Fig. 5. We have assumed two mandatory requirements for a good cavity design: first the existence of a cancellation position Y_p for all models of the support points, and, second, good agreement between the position of the cancellation position Y_p for all models of the support points. Based on these criteria we have excluded geometries with $Z_c<3$ mm as they do not show a cancellation position.

As an additional requirement, the optimum position of the support points, Y_p, where k_z^L=0, must also correspond to low values for all other sensitivity coefficients. Concerning the sensitivity to vertical acceleration, this means that we want to minimize tilt of the mirrors so that k_z^T is vanishingly small. This requirement also means that we want k_x and k_y close to zero. Since symmetries ensure that k_x^L and k_y^L are both zero, we are focused on canceling k_x^T and k_y^T. For each coefficient, the aim was to achieve vibration sensitivity below 10^{-11} (m s^{-2})$^{-1}$ for a putative offset of the optical axis d =1 mm.

With these considerations in mind, we have simulated a large number of geometries and reached the conclusion that X_c=47 mm and Z_c=3 mm was the best compromise. In the following we present the results of the simulation obtained with this optimized geometry, which are also shown in Figs. 5 and 6.

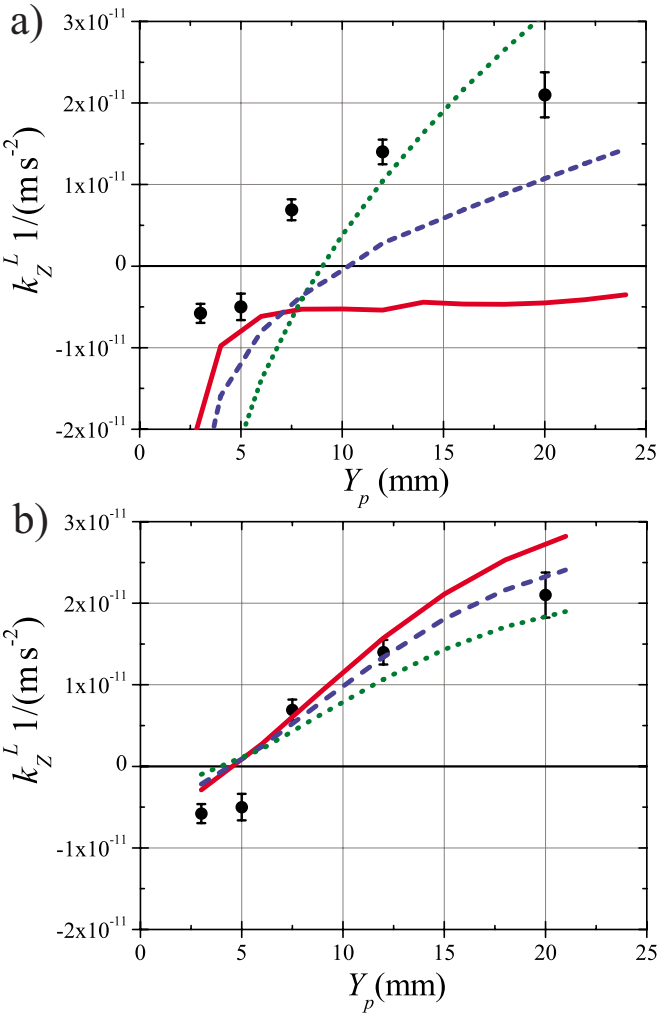

FIG. 5. (Color online) Comparison between measurements and simulation results for the vertical vibration sensitivity (horizontal cavity) as a function of the support points distance from mirror, Y_p. Contact points are (a) totally constrained or (b) vertically constrained with areas of 0.04 mm^2 (red solid line), 1 mm^2 (blue dashed line), and 4 mm^2 (green dotted line). The support points of the cavity are 2 mm^2 (black points).

Figure 5 shows the sensitivity to vertical acceleration k_z^L as a function of the support points' position. Simulations have been performed for a range of contact point sizes for two different models: totally constrained and only vertically constrained. This figure illustrates that for this cavity design, the coefficient k_z^L is strongly dependent on the contact model: the size of the contact points and the constraints placed on the degrees of freedom.

When the contact points are constrained in all directions, a small size gives a very low k_z^L regardless of longitudinal position Y_p of contact points. For larger surface sizes, a solution with k_z^L=0 does exist for $Y_p \approx 10$ mm (Fig. 5). When the contact with the cavity is only vertically constrained, the insensitive solution is independent of the support-point size.

The vertical acceleration also induces tilt in the mirrors but the sensitivity coefficient k_z^T is independent of the contact model. Assuming a rather large misalignment d=1 mm, the

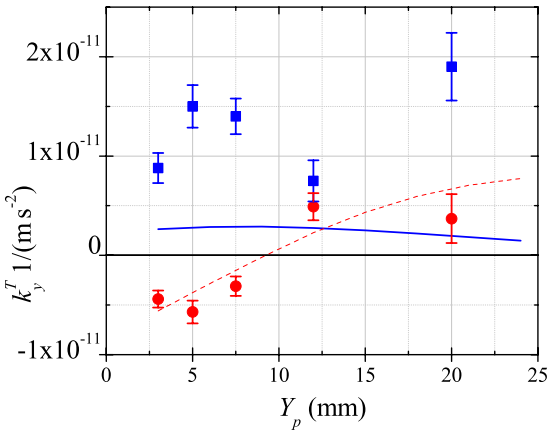

FIG. 6. (Color online) Horizontal vibration sensitivity of the horizontal cavity as a function of Y_p for $d=1$ mm and contact point size of 2 mm^2. Transverse vibration sensitivity measurements k_x^T (red circles) and simulation (red dashed line) and longitudinal vibration sensitivity measurements k_y^T (blue squares) and simulation (blue solid line) are shown.

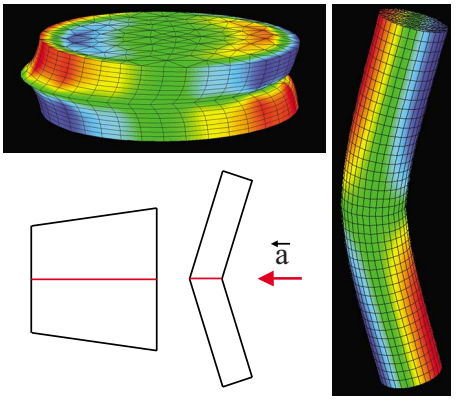

FIG. 8. (Color online) Deformation of a cylinder with ULE properties when acceleration is applied to the center (arrow). For the two different diameter:length ratios, the ends of each cylinder are tilted in different directions (explained in text). Color scale illustrates vertical displacement only, where blue is negative and red is positive with respect to the center of the nondeformed cylinder. Deformations are amplified by a factor of $\approx 10^6$.

dependence on the support-point position is low, $\sim 1.3 \times 10^{-12}$ (m s^{-2})$^{-1}$/mm, with $k_z^T=0$ for $Y_p \sim 10$ mm.

Transverse (k_x) and longitudinal (k_y) components depend on the position of the support points, but are virtually independent of the contact point size (Fig. 6). Note again that due to symmetry, only tilt of the mirrors contributes to both horizontal sensitivities $k_x=k_x^T(d)$ and $k_y=k_y^T(d)$. We find that the transverse component can be zeroed for the support-point positions set at $Y_p \approx 9$ mm with a slope of $\approx 2 \times 10^{-12}$ (m s^{-2})$^{-1}$/mm.

When an axial vibration is applied (k_y), the two mirrors are tilted in the same direction (Fig. 7). The worst misalignment to consider is when the mechanical and optical axes are no longer parallel. In this case, we characterize this by a displacement d of the optical axis on one of the mirrors, and $-d$ on the other. The longitudinal vibration sensitivity component $k_y=k_y^T(d)$ also depends on d. In our chosen geometry,

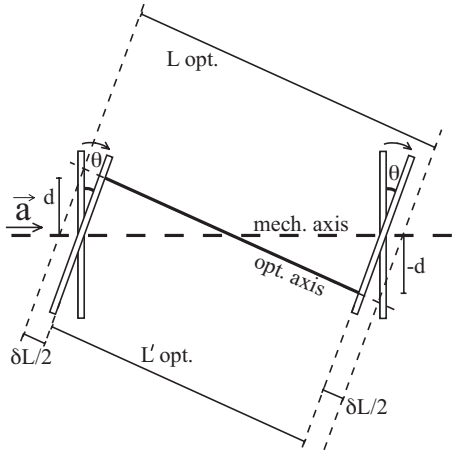

FIG. 7. Schematic showing mirror tilt as a result of applied longitudinal acceleration $\vec{a}$ occurring only in the horizontal cavity. This leads to changes in optical length L, as the mechanical axis and optical axis are misaligned and not parallel.

we have found that this component cannot be zero. However for $d=1$ mm it is always below 3×10^{-12} (m s^{-2})$^{-1}$ and therefore negligible (Fig. 6).

C. Vertical cavity

The vertically mounted cavity geometry is 100 mm long, and the optical axis lies along the z axis (Fig. 2). The contact plane is obtained by machining a central "shoulder" in the spacer. The cavity is constrained by three equidistant support points as shown in Fig. 2. This configuration allows the distribution of equal restoring forces from the support to the cavity.

The cavity has cylindrical symmetry around the optical axis (z axis); therefore k_x^L and k_y^L vanish. Rigorously, the three support points break the rotational symmetry. However, simulation results indicate that this has a negligible effect on vibration sensitivity. The lack of an exact rotational symmetry means that there is no geometry for which k_x^T and k_y^T can simultaneously be zero. The magnitude of the horizontal vibration sensitivity coefficients k_x^T and k_y^T depend on the diameter:length ratio of the spacer.

When the diameter:length ratio is small, the cylinder deformation is dominated by bending about the center. When it is large the deformation induced by the Poisson effect dominates. In each case, the ends of the cylinder are tilted in opposite directions and therefore change the mirror tilt of the cavity (Fig. 8). By choosing the correct ratio, it is possible to cancel out the mirror tilt. Fixing the spacer diameter at 110 mm, simulations indicate that a 100-mm-long spacer is optimal, minimizing both horizontal components k_x^T and k_y^T at $\sim 1 \times 10^{-12}$ (m s^{-2})$^{-1}$ for $d=1$ mm.

The vertical vibration sensitivity component depends on the position of the contact plane and the geometry of the supporting shoulder. This component is nearly vanishing when the contact plane is optimally positioned, in this case 3 mm below the center of the spacer for the chosen geometry of the shoulder as shown in Fig. 2. As a result, length varia-

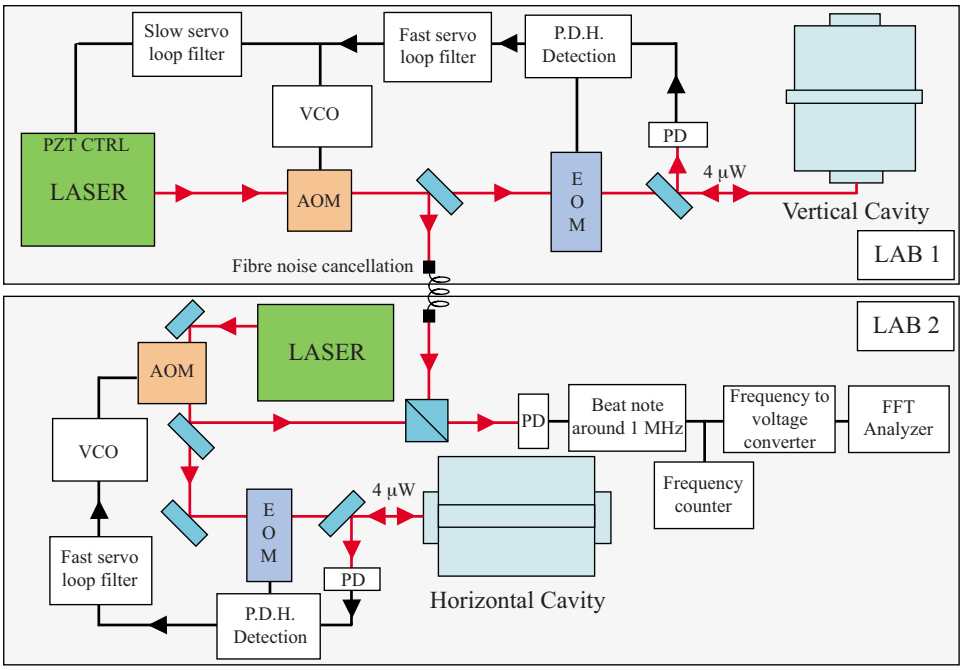

FIG. 9. (Color online) Schematic showing the two independent lasers used to create the beat note with the horizontal and vertical cavities. PDH: Pound Drever Hall setup [20]; PD: photodiode; FFT: fast Fourier transform analyzer; VCO: voltage-controlled oscillator; PZT CTRL: piezoelectric transducer control.

tions in the upper part of the spacer compensate exactly for those of the lower part [18]. Due to this geometry of the spacer and the forces applied, the mirrors are translated without any mirror tilt.

III. EXPERIMENTAL SETUP

Based on the results of these comprehensive simulations, two ultrastable optical cavities have been designed and constructed: one horizontal, and the other vertical.

The spacers of the two cavity configurations are machined from ULE glass rods. The wavelength range of the high-reflection coating mirrors allow operation at both 1064 and 1062.5 nm (Nd:YAG and Yb-doped fiber laser). Each cavity has been optically contacted with a flat mirror and a concave mirror with radius of curvature of 500 mm. Both cavities show a finesse of ≈800 000 and a fringe contrast better than 50%.

The substrates of the mirrors are made from fused silica to reduce the contribution of thermal noise floor [15,19]. For the present geometry, this limit is estimated to have a flicker noise floor of $\approx 4 \times 10^{-16}$ for a 100-mm-long cavity with fused silica mirrors, dominated by the thermal noise of the high-reflection coatings. The expected improvement compared to an all-ULE cavity is greater than a factor of 2 [13,14].

However, fused silica shows a larger coefficient of thermal expansion (CTE) than ULE. Consequently, the overall effective CTE of the cavity is much larger than that of an all-ULE cavity and the zero thermal-expansion coefficient is shifted to well below 0 °C, instead of 10–20 °C for an all-ULE cavity. This increased temperature sensitivity requires a more sophisticated design of the cavity environment. A high thermal shielding factor coupled with a tight temperature control is necessary to minimize the impact of environmental temperature fluctuations.

IV. VIBRATION SENSITIVITY MEASUREMENTS

For both cavities, the three vibration sensitivity components were measured by shaking the cavity setup with sinusoidal signals in the frequency range of 1–10 Hz. Each cavity is housed in a vacuum chamber supported on an optical table in two separate rooms. The horizontal cavity setup (cavity, vacuum chamber, and optical table) is supported by an active vibration isolation platform. The cavity itself is supported under vacuum with four 2 mm^2 Viton pads 0.7 mm thick. The vertical cavity setup is isolated from vibration using a passive isolation table, and is supported under vacuum with the same Viton pads used for the horizontal setup. Air flow, acoustic noise, and large temperature fluctuations are strongly filtered by containing the whole system in a thermoacoustic isolation box. The vacuum chamber temperature is actively stabilized at ≈22 °C.

Two lasers in two different rooms (each with their own air-conditioning system) are independently stabilized to these

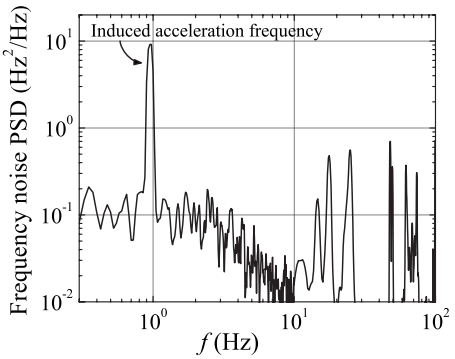

FIG. 10. Frequency noise power spectral density for induced vertical acceleration in the horizontal cavity. Measurement between two lasers locked separately onto the horizontal and the vertical cavities.

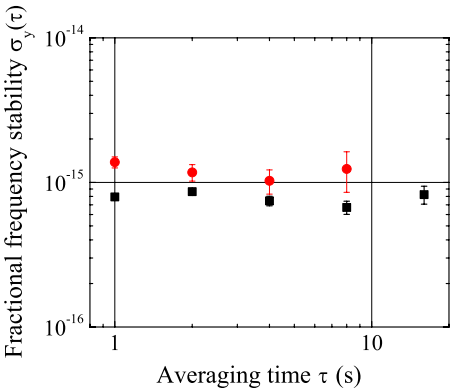

FIG. 11. (Color online) Fractional frequency stability (Allan standard deviation). Red circles' plot: a laser locked onto a vertical cavity at 1062.5 nm against the laser at 698 nm locked onto another vertical cavity. Comparison realized via a Ti:sapphire-based frequency comb. Black squares' plot (10 Hz s^{-1} frequency drift removed): direct beat-note signal between a laser locked onto the horizontal cavity and a laser locked onto the vertical cavity, both at 1062.5 nm.

two cavities using the Pound-Drever-Hall technique. The beat-note signal between the two stable lasers is demodulated by a frequency-to-voltage converter and analyzed with a fast Fourier transform analyzer (Fig. 9).

A low-noise seismometer placed on the top of the vacuum chamber is used to measure the acceleration of the horizontal cavity in three spatial directions. Each of the three orthogonal spatial directions is excited in turn, while the amplitude of the induced frequency tone and the strength of the acceleration are measured. These measurements are iterated for several support-point positions of the horizontal cavity. The active platform can apply accelerations in a given direction with an amplitude of up to 10^{-3} m s^{-2} rms. However, the coupling to other directions could be as much as 10%. A typical frequency response measurement for induced vertical acceleration at 1 Hz can be seen in Fig. 10, with rms value of $\approx 7.5\times10^{-4}$ m s^{-2}. The phase between the frequency response signal (filtered and amplified) and the vibration excitation signal is also measured, and gives the relative sign of the cavity response. Measurement error bars have been estimated by considering the contribution of the signal-to-noise ratio (5%) of the frequency deviation measurements, the acceleration cross-talk effects (6%–10% depending on the axis under consideration), and the calibration error on vibration measurement (5%).

These results for the horizontal cavity measuring the vertical response agree with the vertically constrained model and contact surfaces of about 1 mm^2 (Fig. 5). The lowest vibration sensitivity component observed is 5×10^{-12} $(m\ s^{-2})^{-1}$ and the dependence on the support-point position is very low: 1.6×10^{-12} $(m\ s^{-2})^{-1}/mm$.

The difference between the horizontal sensitivity component measurements and simulations in Fig. 6 can be explained by the unequal restoring forces of the four support points on the cavity. An asymmetry induces length variation and consequently the coefficients k_x^L and k_y^L are no longer equal to zero. This asymmetry is not reproducible when

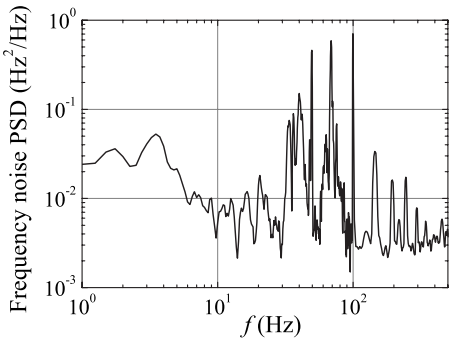

FIG. 12. Frequency noise power spectral density measured between lasers locked separately onto the horizontal and the vertical cavities.

support-point positions are changed and can explain the dispersion of different measurements. However, a linear fit of k_x measured as function of Y_p agrees with coefficients k_x^T simulated for an offset between the mechanical and optical axes of $d=0.3$ mm. The longitudinal vibration sensitivity is most sensitive to asymmetry of the restoring forces. Components measured are four to eight times larger than the coefficient k_y^T simulated, even for a model with a large offset of $d=1$ mm (Fig. 6).

A similar measurement has been performed to estimate the vibration sensitivity component of the vertical cavity. In this case the isolation platform is passive, so sinusoidal accelerations were mechanically induced on the optical table. The results were measured using a piezoaccelerometer, at a drive frequency of 1.2 Hz. All three axes were measured during the acceleration of each direction to check for coupling. In this measurement, sensitivity components obtained were $\sim 3.5\times10^{-12}$ $(m\ s^{-2})^{-1}$ in the vertical direction and 1.4×10^{-11} $(m\ s^{-2})^{-1}$ in both horizontal directions. These results are significantly better than those reported previously [13].

Three other horizontal optical cavities were also constructed to the design specifications presented in this paper. One cavity operates at 698 nm and also has fused silica mirrors, showing finesse of ≈600 000 and a fringe contrast better than 70%. The other two are identical all-ULE cavities operating at 1.55 μm.

V. FREQUENCY STABILITY RESULTS

A comparison between two independent lasers locked on the vertical and the horizontal cavities has already shown the frequency stability to be 7.9×10^{-16} at 1 s and 6.7×10^{-16} at 8 s (Fig. 11, black squares plot). The frequency drift is about 10 Hz s^{-1} due to the incomplete thermal control of the horizontal cavity, which will be largely reduced in future by adding a thermal shield and actively controlling the temperature for this setup. Nevertheless, this demonstrates that at least one of the two lasers exhibits a frequency stability better than 5.6×10^{-16} at 1 s. A measurement of the frequency noise of the beat note (Fig. 9) between lasers stabilized onto the horizontal and vertical cavities is shown in Fig. 12.

These stability results for the horizontal and vertical cavities can be compared with those from a different cavity built to the same design, but with ULE mirrors rather than fused silica. This laser is supported on 1.5 mm Viton pads, but otherwise has the same setup. Frequency stability for the all-ULE cavity is 1.8×10^{-15} at 1 s [6], close to the expected thermal noise limit. This demonstrates the improvement in stability achieved by replacing ULE mirror substrate by fused silica mirror substrate. The red circles plot in Fig. 11 is a measurement of the relative frequency stability between a laser at 1062.5 nm locked onto the vertical fused silica mirror cavity, and the 698 nm laser cavity locked onto the fused silica mirror horizontal cavity. The comparison was realized via a Ti:sapphire-based optical frequency comb [1]. The measured stability is close to 10^{-15} from 1 to 10 s, a level at which we do not exclude contributions from the Ti:sapphire frequency comb noise.

VI. CONCLUSION

Two different optical cavity designs have been studied using simulations with the purpose of decreasing the influence of vibration on the length of the optical axis. These cavity designs have been constructed and their vibration sensitivity has been measured. In addition to the usual study of mirror translation, it is shown that the effect of mirror tilt is of great significance.

For the horizontal cavity, vibration sensitivity is $\approx10^{-11}$ $(\mathrm{m\ s^{-2}})^{-1}$ or better in all directions. The vertical acceleration sensitivity component shows a small dependence on the support-point positions of 1.6×10^{-12} $(\mathrm{m\ s^{-2}})^{-1}/\mathrm{mm}$. Therefore, fine tuning of their positions is not necessary. This is a very important improvement, since fine tuning is a time-consuming and delicate process. Frequency stability will be improved further by optimizing the thermal environment of the horizontal cavity to reduce the observed drift of 10 $\mathrm{Hz\ s^{-1}}$. Measurements also show that the vertical cavity has a low vibration sensitivity, giving 3.5×10^{-12} $(\mathrm{m\ s^{-2}})^{-1}$ in the vertical direction and 1.4×10^{-11} $(\mathrm{m\ s^{-2}})^{-1}$ in the horizontal directions, without any tuning.

The beat-note signal between two independent lasers stabilized to these cavities (vertical and horizontal) shows a frequency stability of 7.9×10^{-16} at 1 s and 6.7×10^{-16} at 8 s (Fig. 11, black squares plot). In contrast to previous studies, the two systems are strongly independent (different cavity designs, different isolation systems, in different rooms), ruling out the possibility of artificial improvements due to correlation between the systems. Therefore, this result demonstrates two ultrastable lasers with stability in the 10^{-16} range, lower than the noise floor of an all-ULE cavity with the same geometry. Consequently this is the best result achieved for a cavity of this length and compactness, potentially suitable for applied systems. This is therefore an unequivocal demonstration of the reduction of thermal noise by the use of fused silica mirrors in an ultrastable cavity design.

[1] T. Rosenband *et al.*, Science **319**, 1808 (2008).
[2] A. D. Ludlow *et al.*, Science **319**, 1805 (2008).
[3] H. Müller, P. L. Stanwix, M. E. Tobar, E. Ivanov, P. Wolf, S. Herrmann, A. Senger, E. Kovalchuk, and A. Peters, Phys. Rev. Lett. **99**, 050401 (2007).
[4] A. Bartels, S. A. Diddams, C. W. Oates, G. Wilpers, J. C. Bergquist, W. H. Oskay, and L. Hollberg, Opt. Lett. **30**, 667 (2005).
[5] P. A. Williams, W. C. Swann, and N. R. Newbury, J. Opt. Soc. Am. B **25**, 1284 (2008).
[6] H. Jiang *et al.*, J. Opt. Soc. Am. B **25**, 2029 (2008).
[7] F. Acernese, Class. Quantum Grav. **23**, S635 (2006).
[8] S. J. Waldman, Class. Quantum Grav. **23**, S653 (2006).
[9] K. Danzmann and A. Rudiger, Class. Quantum Grav. **20**, S1 (2003).
[10] A. Quessada, R. P. Kovacich, I. Courtillot, A. Clairon, G. Santarelli, and P. Lemonde, J. Opt. B: Quantum Semiclassical Opt. **5**, S150 (2003).
[11] T. Rosenband and J. Bergquist (private communication).
[12] T. Nazarova, F. Riehle, and U. Sterr, Appl. Phys. B: Lasers Opt. **83**, 531 (2006).
[13] A. D. Ludlow, X. Huang, M. Notcutt, T. Zanon-Willette, S. M. Foreman, M. M. Boyd, S. Blatt, and J. Ye, Opt. Lett. **32**, 641 (2007).
[14] S. A. Webster, M. Oxborrow, and P. Gill, Phys. Rev. A **75**, 011801 (2007).
[15] K. Numata, A. Kemery, and J. Camp, Phys. Rev. Lett. **93**, 250602 (2004).
[16] S. A. Webster, M. Oxborrow, S. Pugla, J. Millo, and P. Gill, Phys. Rev. A **77**, 033847 (2008).
[17] S. D. Poisson, *A Treatise of Mechanics* (Longman, London, 1842).
[18] C. T. Taylor, M. Notcutt, and D. G. Blair, Rev. Sci. Instrum. **66**, 955 (1995).
[19] M. Notcutt, L.-S. Ma, A. D. Ludlow, S. M. Foreman, J. Ye, and J. L. Hall, Phys. Rev. A **73**, 031804 (2006).
[20] R. W. P. Drever, J. L. Hall, F. V. Kowalski, J. Hough, G. M. Ford, A. J. Munley, and H. Ward, Appl. Phys. B: Lasers Opt. **31**, 97 (1983).